Chinese Journal of Natural Medicines

Xanthones from *Garcinia pedunculata* and *Garcinia nujiangensis* and their anti-inflammatory activity

Xiaojie Fan, Yufeng Jia, Jiaxin Guo, Jinyuan Yang, Dahong Li, Huiming Hua

Citation: Xiaojie Fan, Yufeng Jia, Jiaxin Guo, Jinyuan Yang, Dahong Li, Huiming Hua, Xanthones from *Garcinia pedunculata* and *Garcinia nujiangensis* and their anti-inflammatory activity, Chinese Journal of Natural Medicines, 2025, 23(2), 225-233. doi: 10.1016/S1875-5364(25)60826-0.

View online: https://doi.org/10.1016/S1875-5364(25)60826-0

Chinese Journal of Natural Medicines 23 (2025) 225-233

Contents lists available at ScienceDirect

Chinese Journal of Natural Medicines

journal homepage: www.cjnmcpu.com/

Original article

Xanthones from *Garcinia pedunculata* and *Garcinia nujiangensis* and their anti-inflammatory activity

Xiaojie Fan, Yufeng Jia, Jiaxin Guo, Jinyuan Yang, Dahong Li*, Huiming Hua*

Key Laboratory of Structure-Based Drug Design & Discovery, Ministry of Education, and School of Traditional Chinese Materia Medica, Shenyang Pharmaceutical University, Shenyang 110016, China

ARTICLE INFO

Article history:
Received 8 May 2024
Revised 29 June 2024
Accepted 1 August 2024
Available online 20 February 2025

Keywords:
Garcinia pedunculata
Garcinia nujiangensis
Xanthones
Network pharmacology
Anti-inflammation

ABSTRACT

Ten novel xanthones, garpedunxanthones A–G (**1**–**5**, **6a**/**6b**, **7a**/**7b**) and nujiangxanthone Q (**8**), along with sixteen known analogs (**9**–**24**), were isolated from *Garcinia pedunculata* and *G. nujiangensis*. Their structures were elucidated through high-resolution electrospray ionization mass spectrometry (HR-ESI-MS) data, comprehensive nuclear magnetic resonance (NMR) spectroscopic analyses, and electronic circular dichroism (ECD) calculations. All compounds without cytotoxicity were assessed for anti-inflammatory properties by measuring the inhibition of nitric oxide (NO) production in lipopolysaccharide (LPS)-induced RAW264.7 cells. Structure-activity relationships are also discussed. Compounds **7b**, **19**, and **21** exhibited significant anti-inflammatory activity with IC_{50} values of 16.44 ± 0.69, 14.28 ± 0.78, and 10.67 ± 3.28 μmol·L^{-1}, respectively. Enzyme-linked immunosorbent assay (ELISA) demonstrated that compounds **7b**, **19**, and **21** inhibited the expression of pro-inflammatory cytokines TNF-α and IL-6 in a dose-dependent manner. The inhibitory effect of compound **21** on IL-6 at 20 μmol·L^{-1} was comparable to that of the positive control. In network pharmacology studies, potential targets of compounds and inflammation were identified from PharmMapper and GeneCards databases. Gene Ontology (GO) and Kyoto Encyclopedia of Genes and Genomes (KEGG) enrichment analysis revealed that the overlapped targets were intricately associated with major pathogenic processes linked to inflammation, including positive regulation of mitogen-activated protein kinase (MAPK) cascade, protein kinase activity, NO synthase regulator activity, MAPK signaling pathway, and EGFR tyrosine kinase inhibitor resistance.

1. Introduction

Inflammation is a physiological response that activates the immune system when the body experiences injury [1]. Chronic inflammation is associated with cellular damage, which can lead to the development of various diseases, including cancer, diabetes, and cardiovascular disorders [2]. The current approach to mitigate inflammation primarily involves regulating the secretion of inflammatory cytokines through established signaling pathways. Cytokines play a crucial role in the immune system, and elevated nitric oxide levels are associated with nitric oxide synthase, a pro-inflammatory factor essential in various inflammatory cells [3]. Lipopolysaccharide (LPS) is a complex of lipids and polysaccharides that specifically stimulates macrophages to promote the secretion of pro-inflammatory cytokines, such as nitric oxide (NO), IL-6, IL-1β and TNF-α [4], as well as inflammatory mediators like INOS and COX-2 [5]. However, due to the significant side effects and drug resistance associated with existing anti-inflammatory medications, there is an urgent need to explore and develop novel anti-inflammatory therapeutics.

The *Garcinia* genus, belonging to the Guttiferae family, comprises 450 species worldwide, distributed across tropical Asia, Southern Africa, and Western Polynesia. In China, 21 species are present, primarily in Southern Taiwan, Southern Guangxi, and Yunnan. *Garcinia* plants have been extensively studied in phytochemistry and biological activity. The chemical constituents of this genus mainly include xanthones, phloroglucinols, biphenyls, and flavonoids. Previous research has demonstrated that these compounds exhibit a broad spectrum of biological activities, including anti-tumor [6], anti-inflammatory [7], and antihyperlipidemic effects [8]. In India, *G. pedunculata* is utilized as a folk medicinal plant for treating gastrointestinal diseases [9]. *G. pedunculata*, also known as slimming fruit, contains significant amounts of hydroxycitric acid, which can inhibit fat synthesis [10]. The medicinal efficacy of *G. nujiangensis* remains unreported and requires further investigation. Currently, limited research exists on the chemical composition and biological activity of *G. pedunculata* and *G. nujiangensis*, with isolated compounds primarily including benzophenones, xanthones, and other compounds. A systematic study was undertaken to investigate the components of *G. pedunculata* and *G. nujiangensis* to discover novel anti-inflammatory xanthones as potential active leads. This effort resulted in the isolation of ten previously undescribed xanthones (**1**–**5**, **6a**/**6b**, **7a**/**7b**, and **8**) and sixteen known analogs (**9**–**24**) (Fig. 1). All compounds were evaluated for their effects on cell viability and

* Corresponding author.
E-mail addresses: lidahong0203@163.com (D. Li); huimhua@163.com (H. Hua)

https://doi.org/10.1016/S1875-5364(25)60826-0

anti-inflammatory properties by measuring the inhibition of NO production in LPS-stimulated RAW264.7 macrophages. Furthermore, the pro-inflammatory cytokine (TNF-α and IL-6) content of compounds exhibiting significant anti-inflammatory activity was quantified. Their potential anti-inflammatory mechanism was predicted through network pharmacology studies. This paper reports the isolation, structure elucidation, bioactivities, and structure-activity relationships of these compounds.

2. Results and discussion

Compound **1** was isolated as a pale yellow amorphous powder. Its molecular formula was determined to be $C_{23}H_{18}O_6$ by high-resolution electrospray ionization mass spectrometry (HR-ESI-MS) ([M − H]$^-$ at *m/z* 389.1025, Calcd. for $C_{23}H_{17}O_6$, 389.1025), indicating 15 degrees of unsaturation (DOU). The ultraviolet spectrum exhibited maximum absorption at λ_{max} 283 and 350 nm, suggesting a xanthone analog structure [11]. The ^{1}H nuclear magnetic resonance (NMR) (Table 1), ^{13}C NMR (Table 2), and heteronuclear single quantum coherence (HSQC) spectra revealed signals for a chelated hydroxyl [δ_H 13.92 (1H, s, OH-1)], two isolated aromatic protons [δ_H 6.39 (1H, s, H-4), 6.62 (1H, s, H-5)], a 2,2-dimethyl-pyran ring fragment [δ_H 6.61 (1H, d, *J* = 10.0 Hz, H-1'), 5.74 (1H, d, *J* = 10.0 Hz, H-2'), 1.42 (6H, s, CH_3-4', 5'), and δ_C 128.1 (C-2'), 114.7 (C-1'), 77.9 (C-3'), 27.8 × 2 (C-4', 5')], and a 2-(1-methylvinyl)-furan ring fragment [δ_H 7.52 (1H, s, H-1''), 5.78 (1H, s, H-4a''), 5.29 (1H, s, H-4b''), 2.14 (3H, s, CH_3-5'') and δ_C 158.1 (C-2''), 132.5 (C-3''), 114.1 (C-4''), 104.9 (C-1''), 19.0 (C-5'')]. Apart from the carbon signals assigned to 2,2-dimethyl-pyran and 2-(1-methylvinyl)-furan, the ^{13}C NMR spectrum displayed 12 aromatic and one carbonyl carbon signals attributed to a xanthone skeleton. Based on the heteronuclear multiple bond correlation (HMBC) cross-peaks (Fig. 2) from the chelated hydroxyl at δ_H 13.92 to C-1 (δ_C 156.6), C-2 (δ_C 103.7), the hydroxyl was assigned to C-1. The olefinic proton signal at δ_H 6.61 of the 2,2-dimethyl-pyran ring showed cross-peaks with C-1 (δ_C 156.6), C-2 (δ_C 103.7), C-3 (δ_C 158.7), C-3' (δ_C 77.9), and the one at δ_H 5.74 showed cross-peaks with C-2 (δ_C 103.7), C-3' (δ_C 77.9), C-4' (δ_C 27.8) in the HMBC spectrum, locating the 2,2-dimethyl-pyran ring fragment fused with C-2 and C-3 of the xanthone core. The aromatic proton at δ_H 6.39 was assigned to C-4 based on the HMBC from the proton to C-2 (δ_C 103.7), C-3 (δ_C 158.7), C-4a (δ_C 156.1), and C-9a (δ_C 102.6). Another aromatic proton at δ_H 6.62 was assigned to C-5 by its correlations to C-7 (δ_C 141.5), C-8a (δ_C 103.0), and C-10a (δ_C 155.8). The downfield shifted olefinic proton signal at δ_H 7.52 suggested that the 2-(1-methylvinyl)-furan ring was linked at C-8, confirmed by the cross-peaks between the proton and C-7 (δ_C 141.5), C-8 (δ_C 126.3), C-2'' (δ_C 158.1), and C-3'' (δ_C 132.5). The NMR data (Tables 1 and 2) of **1** at the ring A unit were similar to those of cudratrianthone O [12], supporting the furan ring fused with ring A at C-7 and C-8. Consequently, the structure of **1** was elucidated as shown and named garpedunxanthone A.

Compound **2** was isolated as a yellow needle crystal. The HR-ESI-MS analysis of **2** revealed an ion at *m/z* 351.0863 [M + H]$^+$ (Calcd. for $C_{20}H_{15}O_6$, 351.0869), indicating a molecular formula of $C_{20}H_{14}O_6$ with 14 DOU. The ultraviolet absorption at λ_{max} 284 and 337 nm suggested that compound **2** could be a xanthone derivative. Comparison of the ^{1}H NMR (Table 1) and ^{13}C NMR (Table 2) spectra of **2** and **1** indicated their structural similarity, with the notable absence of a methylvinyl moiety at C-2'' in **2**. The substitution pattern of **2** was elucidated through comprehensive HMBC analysis, with key correlations depicted in Fig. 2. Consequently, the structure of **2** was established and designated as garpedunxanthone B. This novel compound was isolated for the first time, previously observed only as a fragment ion in the mass spectral fragmentation pathway of 9-hydroxycalabaxanthone [13].

Compound **3** was isolated as a pale yellow amorphous powder with a molecular formula of $C_{23}H_{22}O_6$, having four mass units less than **1**. This was confirmed by HR-ESI-MS ([M + H]$^+$ at *m/z* 395.1489, Calcd. for $C_{23}H_{23}O_6$, 395.1495). The ultraviolet spectrum (λ_{max} 290 and 338 nm) indicated a potential xanthone derivative. Comparison of ^{1}H NMR (Table 1) and ^{13}C NMR (Table 2) data between **3** and **1** revealed close structural similarities, with the main difference being the replacement of a 2-(1-methylvinyl)-furan ring in **1** by a 2-isopropyl-2,3-dihydrofuran ring in **3**. The ^{1}H-^{1}H COSY spectrum (Fig. 2) demonstrated a spin coupling system, -CH_2-CH-CH-$(CH_3)_2$- [δ_H 4.66 (1H, dd, *J* = 15.7, 8.9 Hz, H-2''), 3.72 (1H, dd, *J* = 17.2, 9.3 Hz, H-1''b), 3.39 (1H, dd, *J* = 17.2, 8.8 Hz, H-1''a), 2.00 (1H, m, H-3''), 1.07 (3H, d, *J* = 6.6 Hz, CH_3-4''), 1.02 (3H, d, *J* = 6.6 Hz, CH_3-5'')]. The observed HMBC (Fig. 2) from the proton at δ_H 3.39 to C-7 (δ_C 147.1), C-8 (δ_C

Table 1 ^{1}H NMR (600 MHz) data of compounds **1**–**5**

No.	**1**[a]	**2**[a]	**3**[b]	**4**[a]	**5**[a]
	δ_H (*J* in Hz)	δ_H (*J* in Hz)	δ_H (*J* in Hz)	δ_H (*J* in Hz)	δ_H (*J* in Hz)
4	6.39, s	6.40, s	6.21, s	6.30, s	6.31, s
5	6.62, s	6.71, s	6.61, s	6.68, s	6.65, s
1'	6.61, d (10.0)	6.61, d (10.0)	6.65, d (10.0)	6.60, d (10.0)	6.59, d (10.0)
2'	5.74, d (10.0)	5.74, d (10.0)	5.64, d (10.0)	5.71, d (10.0)	5.71, d (10.0)
4'	1.42, s	1.42, s	1.45, s	1.41, s	1.41, s
5'	1.42, s	1.42, s	1.44, s	1.41, s	1.41, s
1''	7.52, s	7.59, d (1.8)	3.39, dd (17.2, 8.8) 3.72, dd (17.2, 9.3)	4.07, d (7.2)	
2''		8.19, d (1.8)	4.66, dd (15.7, 8.9)	5.47, t (7.2)	2.89, s
3''			2.00, m		
4''	5.78, brs 5.29, brs		1.07, d (6.6)	4.79, s	1.41, s
5''	2.14, s		1.02, d (6.6)	1.64, s	1.41, s
7''				2.04, s	
OH-1	13.92, s	13.79, s		14.12, s	13.36, s

[a] The solvent was DMSO-d_6; [b] The solvent was CD_3OD.

Table 2 ^{13}C NMR (150 MHz) data of compounds **1**–**5**

No.	**1**[a]	**2**[a]	**3**[b]	**4**[a]	**5**[a]
1	156.6	156.6	158.5	157.0	156.2
2	103.7	103.7	105.1	103.4	103.3
3	158.7	158.8	161.0	158.7	158.9
4	94.3	94.4	95.4	93.5	94.1
4a	156.1	156.1	158.4	155.5	155.3
5	99.4	98.7	103.5	100.1	105.8
6	149.4[*]	152.2	151.4	[#]	154.4
7	141.5	141.5	147.1	141.7	148.5
8	126.3	125.2	126.5	125.2	118.3
8a	103.0	103.9	110.7	108.9	108.3
9	178.9	179.3	182.1	181.3	177.6
9a	102.6	102.7	104.3	102.9	104.0
10a	155.8	155.7	154.2	152.4	153.0
1'	114.7	114.6	116.3	114.8	114.6
2'	128.1	128.1	128.5	127.8	128.4
3'	77.9	77.9	79.0	77.8	78.0
4', 5'	27.8	27.8	28.6	27.8	27.8
1''	104.9	108.3	35.7	25.0	190.2
2''	158.1	148.3	91.2	126.8	49.6
3''	132.5		34.6	129.0	81.7
4''	114.1		18.0	63.0	26.5
5''	19.0		28.6	21.2	26.5
6''				170.4	
7''				20.6	

[a] The solvent was DMSO-d_6; [b] The solvent was CD_3OD; [*] In DMSO-d_6+1 ‰TFA; [#] The signal was not observed.

126.5), C-2'' (δ_C 91.2), and C-3'' (δ_C 34.6) confirmed the cyclization of the -CH_2-CH-CH-(CH_3)$_2$- segment at C-7 and C-8 of the xanthone skeleton. This evidence supports the presence of a 2-isopropyl-2,3-dihydrofuran ring fragment. Consequently, the planar structure of **3** was established and named garpedunxanthone C. The compound is racemic, as evidenced by its near-zero specific rotation and flat electronic circular dichroism (ECD) curve. However, due to its limited quantity, separation using a chiral column was not feasible.

Compound **4**, a pale yellow amorphous powder, exhibited a molecular formula of $C_{25}H_{24}O_8$ with 14 DOU, as determined by HR-ESI-MS ([M − H]$^-$ at *m/z* 451.1403, Calcd. for $C_{25}H_{23}O_8$, 451.1393). The UV spectrum revealed maximum absorption peaks at 292 and 335 nm. NMR spectra (Tables 1 and 2) indicated the presence of a chelated hydroxyl group at δ_H 14.12 (1H, s, OH-1), a chelated carbonyl at δ_C 181.3 (C-9), two isolated aromatic methines [δ_H 6.30 (1H, s, H-4), 6.68 (1H, s, H-5) and δ_C 93.5 (C-4), 100.1 (C-5)], a 2,2-dimethyl-pyran ring fragment [δ_H 6.60 (1H, d, *J* = 10.0 Hz, H-1') , 5.71 (1H, d, *J* = 10.0 Hz, H-2'), 1.41 (6H, s, CH_3-4', 5'); δ_C 127.8 (C-2'), 114.8 (C-1'), 77.8 (C-3'), 27.8 × 2 (C-4', 5')], and a 3-acetoxymethyl-2-butene group [δ_H 5.47 (1H, t, *J* = 7.1 Hz, H-2''), 4.79 (2H, s, CH_2-4''), 4.07 (2H, d, *J* = 7.2 Hz , H-1''), 2.04 (3H, s, CH_3-7''), 1.64 (3H, s, CH_3-5''); δ_C 129.0 (C-3''), 126.8 (C-2''), 25.0 (C-1''), 63.0 (C-4''), 21.2 (C-5''), 170.4 (C-6''), 20.6 (C-7''). The NMR data of **4** were comparable to those of 7-*O*-demethyl mangostanin [14]. The primary difference was an additional acetoxymethyl [δ_H 4.79 (2H, s, CH_2-4''), 2.04 (3H, s, CH_3-7''); δ_C 63.0 (C-4''), 170.4 (C-6''), 20.6 (C-7'')] in place of one methyl of isoprenyl in 7-*O*-demethyl mangostanin. The position of the acetoxymethyl at C-3'' was confirmed by HMBC (Fig. 2) between the protons at δ_H 4.79 (2H, s, CH_2-4'') and C-2'' (δ_C 126.8), C-3'' (δ_C 129.0), C-5'' (δ_C 21.2), C-6'' (δ_C 170.4); and at δ_H 2.04 (3H, s, CH_3-7'') and C-6'' (δ_C 170.4). The double bond at C-2'' and C-3'' was determined to be *Z*-type, based on the nuclear Overhauser effect spectroscopy (NOESY) correlation of two protons at δ_H 4.79/4.07. Consequently, the structure of **4** was elucidated and named garpedunxanthone D.

Compound **5** was isolated as a pale yellow amorphous powder. HR-ESI-MS analysis of **5** revealed an ion at *m/z* 407.1131 [M − H]$^-$ (Calcd. for $C_{23}H_{19}O_7$, 407.1131), indicating a molecular formula of $C_{23}H_{20}O_7$ with 14 DOU. UV spectroscopy showed absorption bands at λ_{max} 279 and 393 nm. The ^{1}H NMR spectrum (Table 1) displayed a chelated hydroxyl signal at δ_H 13.36 (1H, s, OH-1) and two isolated aromatic protons at δ_H 6.31 (1H, s, H-4) and 6.65 (1H, s, H-5). The ^{13}C NMR spectrum exhibited 13 carbon signals, including a carbonyl at δ_C 177.6 (C-9) attributed to the xanthone skeleton. Furthermore, the ^{1}H NMR and ^{13}C NMR (Table 2) spectra indicated the presence of a 2,2-dimethyl-pyran fragment [δ_H 6.59 (1H, d, *J* = 10.0 Hz, H-1'), 5.71 (1H, d, *J* = 10.0 Hz, H-2'), 1.41 (6H, s, CH_3-4', 5'); δ_C 128.4 (C-2'), 114.6 (C-1'), 78.0 (C-3'), 27.8 × 2 (C-4'', 5'')], and a 2,2-dimethyl-4-oxo-3,4-dihydropyran group [δ_H 2.89 (2H, s, H-2''), 1.41 (6H, s, CH_3-4'', 5''); δ_C 190.2 (C-1''), 81.7 (C-3''), 49.6 (C-2''), 26.5 × 2 (CH_3-4'', 5''). The NMR data of **5** closely resembled those of garcimangosx-

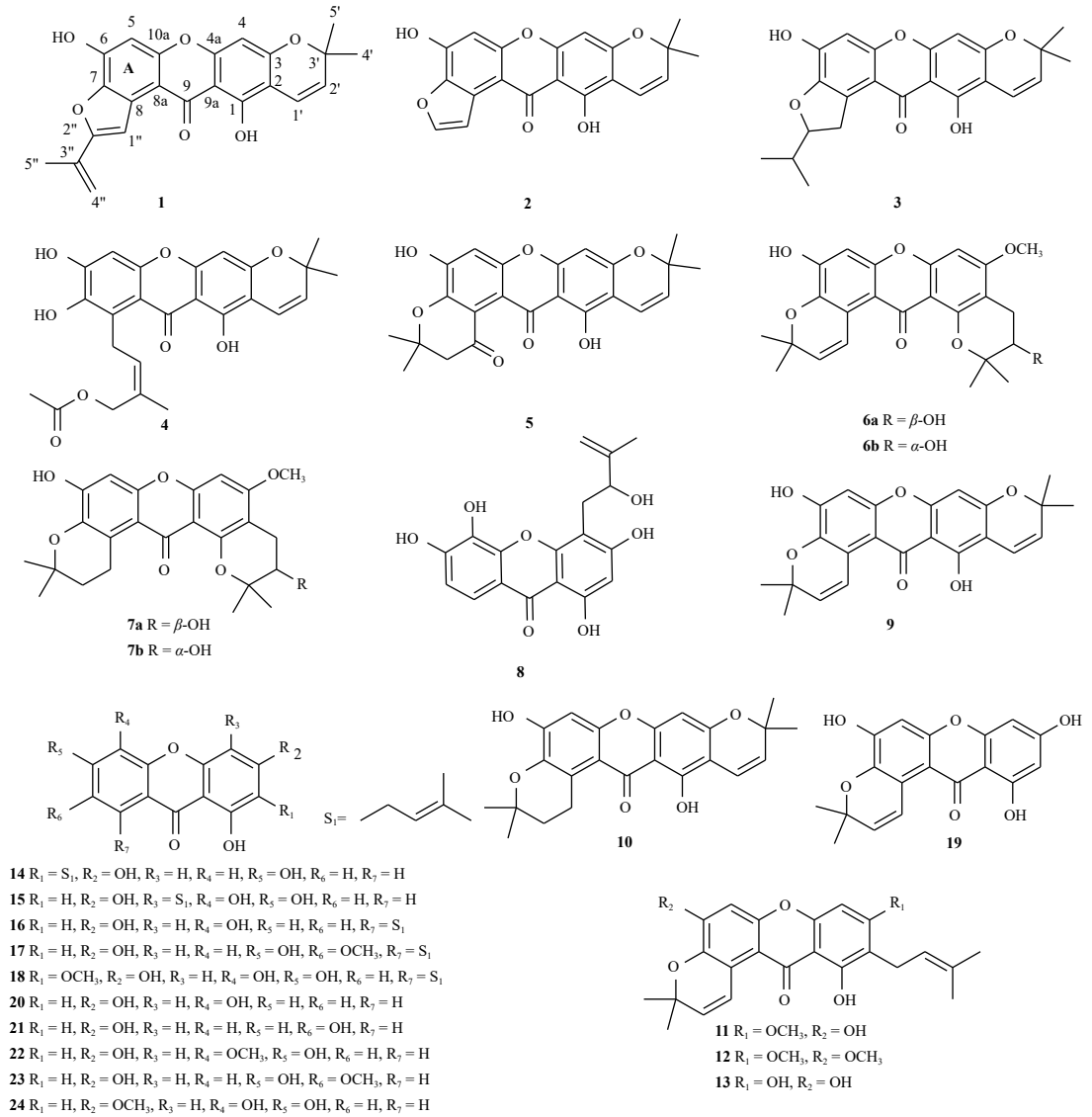

Fig. 1 Chemical structures of compounds **1**–**24**.

anthone D (**10**) [15], with the primary difference being an additional carbonyl [δ_C 190.2 (C-1'')] in place of one methylene of the 2,2-dimethyl-dihydropyran ring in compound **12**. In the HMBC (Fig. 2) spectrum, the methylene proton signal at δ_H 2.89 exhibited cross-peaks with C-8 (δ_C 118.3), C-1'' (δ_C 190.2), C-3'' (δ_C 81.7), and the methyl proton at δ_H 1.41 showed cross-peaks with C-2'' (δ_C 49.6), C-3'' (δ_C 81.7), placing the 2,2-dimethyl-4-oxo-dihydropyran group at C-7 and C-8 of the xanthone core. Consequently, the structure of **5** was elucidated and designated as garpedunxanthone E.

Compound **6** was isolated as a yellow amorphous powder. Its molecular formula was determined to be $C_{24}H_{24}O_7$ by HR-ESI-MS ($[M + H]^+$ at *m/z* 425.1595, Calcd. for $C_{24}H_{25}O_7$, 425.1600), indicating 13 DOU. The ultraviolet spectrum with λ_{max} at 262, 317, and 369 nm suggested that the compound might be a xanthone analog. The ^{1}H NMR and ^{13}C NMR spectra (Table 3) revealed the presence of two isolated aromatic methines [δ_H 6.71 (1H, s, H-5), 6.53 (1H, s, H-4), and δ_C 103.1 (C-5), 91.4 (C-4)], a methoxyl group [δ_H 3.93 (3H, s, OCH_3-3), δ_C 56.5 (OCH_3-3)], a 2,2-dimethyl-pyran fragment [δ_H 7.94 (1H, d, *J* = 10.0 Hz, H-1'') , 5.83 (1H, d, *J* = 10.0 Hz, H-2''), 1.46 (6H, s, CH_3-4'', 5''); δ_C 132.9 (C-2''), 122.4 (C-1''), 76.6 (C-3''), 27.1 × 2 (C-4'', 5'')], and a 2,2-dimethyl-3-hydroxyl-3,4-dihydropyran group [δ_H 3.77 (1H, t, *J* = 7.0 Hz, H-2'), 2.89 (1H, dd, *J* = 17.0, 5.5 Hz, H-1'a), 2.54 (1H, dd, *J* = 17.0, 7.4 Hz, H-1'b), 1.44 (3H, s, CH_3-5'), 1.33 (3H, s, CH_3-4'); δ_C 79.2 (C-3'), 69.4 (C-2'), 26.9 (C-1'), 25.5 (CH_3-5'), 20.6 (CH_3-4')]. The NMR data of **6** were similar to those of garcinoxanthone G [16] with the difference being a methoxyl instead of one hydroxyl in garcinoxanthone G. The positions of all substituents were determined by detailed analysis of the HMBC and HSQC spectra (Fig. 2). The location of the 2,2-dimethyl-3-hydroxyl-dihydro-pyran group was assigned at C-1 and C-2 based on the HMBC correlations from the protons at δ_H 2.89, 2.54 to C-1 (δ_C 155.4), C-2 (δ_C 106.0), and C-2' (δ_C 69.4), along with from δ_H 3.77 to C-2 (δ_C 106.2). The methoxyl proton at δ_H 3.93 showed a cross-peak with C-3 (δ_C 163.5), locating the methoxyl at C-3. The HMBC from the olefin proton [δ_H 7.94 (1H, d, *J*=10.0 Hz, H-1'')] to C-7 (δ_C 139.5), and C-3'' (δ_C 76.6) suggested that the 2,2-dimethyl-pyran ring was located at C-7 and C-8. Its specific rotation is near zero, suggesting that it might be racemic. It was separated using high-performance liquid chromatography (HPLC) with a chiral column to obtain **6a/6b**. Their absolute configuration was determined by comparing the experimental ECD with the calculated one. The experimental ECD spectrum of **6a/6b** was in accordance with the calculated ECD curve (Fig. 3A) for 2'*R*/2'*S*, respectively, thus establishing the absolute configuration of compounds **6a/6b**. Therefore, the structures of **6a/6b** were assigned and named (+) and (−) garpedunxanthone F, respectively.

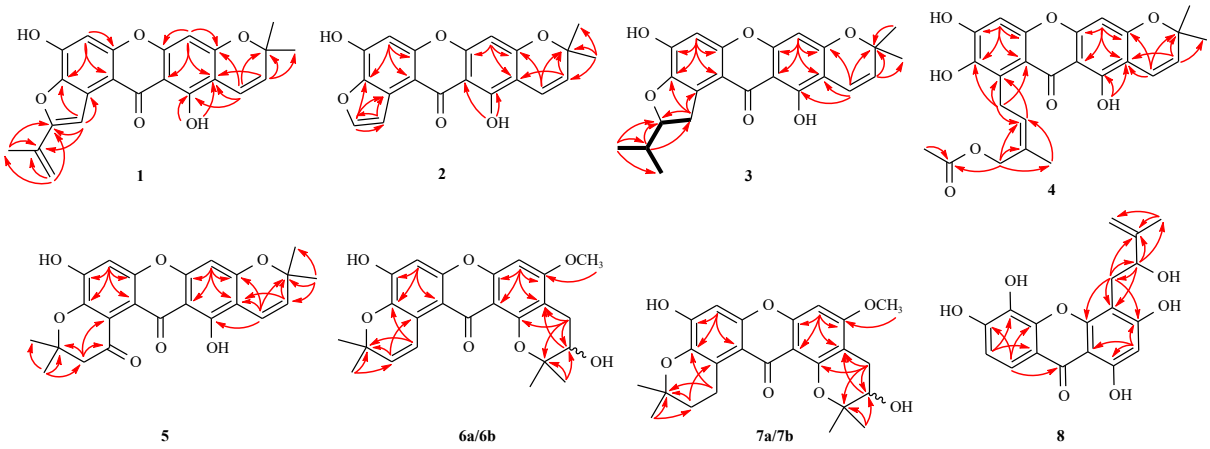

Fig. 2 Key HMBC (red arrows) and ^{1}H-^{1}H COSY (black bold) correlations of compounds **1**–**8**.

Compound **7** was isolated as a yellow amorphous powder with a molecular formula of $C_{24}H_{24}O_7$ and 12 DOU, as determined by HR-ESI-MS ([M + H]$^+$ at *m/z* 427.1751, Calcd. for $C_{24}H_{25}O_7$, 427.1757). The UV spectrum exhibited absorption bands at λ_{max} 256, 306, and 352 nm. Comparison of the ^{1}H NMR and ^{13}C NMR data (Table 3) of **7** with those of **6** indicated a close structural relationship, with the primary difference being the replacement of a 2,2-dimethyl-pyran in **6** by a 2,2-dimethyl-dihydropyran in **7**. The positions of all substituents were confirmed through HMBC (Fig. 2). HMBC cross-peaks from the methylene protons [δ_H 3.45 (2H, t, *J* = 6.8 Hz, H-1'')] to C-7 (δ_C 140.5), C-3'' (δ_C 75.2) indicated that the 2,2-dimethyl-dihydropyran ring was fused with the xanthone skeleton at C-7 and C-8. Compound **7** displayed a near-zero specific rotation, suggesting that it might be racemic. Chiral HPLC separation yielded **7a**/**7b**. The experimental ECD spectra of **7a**/**7b** aligned with the calculated ECD curves (Fig. 3B) for 2'*R*/2'*S*, respectively, thus establishing the absolute configuration of compounds **7a**/**7b**. Consequently, the structures of **7a**/**7b** were assigned as shown and named (+) and (−) garpedunxanthone G, respectively.

Compound **8** was isolated as a yellow amorphous powder. Its HR-ESI-MS displayed an ion at *m/z* 343.0819 [M − H]$^-$ (Calcd. for $C_{18}H_{15}O_7$, 343.0818), indicating 13 DOU. The ultraviolet spectrum with λ_{max} at 252 and 327 nm suggests a xanthone structure. The ^{1}H NMR spectrum (Table 4) revealed a pair of *ortho*-coupled aromatic protons [δ_H 6.87 (1H, d, *J* = 7.9 Hz, H-7), 7.57 (1H, d, *J* = 7.9 Hz, H-8)], an isolated aromatic proton [δ_H 6.21 (1H, s, H-2)], and a set of proton signals belonging to a 2-hydroxy-3-methylbutyl-3-en fragment [δ_H 4.48 (1H, t-like, *J* = 6.4 Hz, H-2'), 4.80 (1H, brs, H-4'a), 4.71 (1H, brs, H-4'b), 3.21 (1H, dd, *J* = 13.8, 5.4 Hz, H-1'a), 3.08 (1H, dd, *J* = 13.8, 7.4 Hz, H-1'b), 1.89 (3H, s, CH_3-5')]. The ^{13}C NMR spectrum exhibited 13 carbon signals attributed to the xanthone skeleton and a set of signals [δ_C 148.8 (C-3'), 110.9 (C-4'), 76.3 (C-2'), 29.9 (C-1'), 18.1 (C-5')] corresponding to the 2-hydroxy-3-methylbutyl-3-en moiety. The NMR data (Table 4) of **8** closely resembled those of ugaxanthone [17]. The primary difference was the presence of a 2-hydroxy-3-methylbutyl-3-alkenyl group instead of an isoprenyl group in ugaxanthone. The HMBC (Fig. 2) from the methylene protons at δ_H 3.21, 3.08 to C-3 (δ_C 165.3), C-4 (δ_C 105.6), C-4a (δ_C 157.0), and C-2' (δ_C 76.3), and from the methine proton at δ_H 4.48 to C-4 (δ_C 105.6) and C-1' (δ_C 29.9) indicated that the 2-hydroxy-3-methylbutyl-3-alkenyl group was attached at C-4. The downfield shift of the aromatic proton at δ_H 7.57 in compound **8** suggested two *ortho*-coupled aromatic protons on C-7 and C-8. Consequently, the structure of **8** was established as shown and designated as nujiangxanthone Q.

Through comparison of NMR spectral data with literature reports, the known compounds were identified as brasilixanthone B (**9**) [18], garcimangosxanthone D (**10**) [15], dulcisxanthone F (**11**) [19], 11-hydroxy-5,9-dimethoxy-3,3-dimethyl-10-(3-methyl-2-buten-1-yl)-pyrano[3,2-*a*]xanthen-12(3*H*)-one (**12**) [20], garcinone B (**13**) [20], 1,3,7-trihydroxy-2-(3-methylbut-2-enyl)-xanthone (**14**) [21], 1,3,5-trihydroxy-4-prenylxanthone (**15**) [22], 1,3,5-trihydroxy-8-isoprenylxanthone (**16**) [23], dulxanthone D (**17**) [24], nujiangxanthone M (**18**) [25], toxyloxanthone B (**19**) [24], 1,3,5-trihydroxy-xanthone

Table 3 ^{1}H (600 MHz) and ^{13}C NMR (150 MHz) data of compounds **6** and **7** (in CD_3OD)

No.	**6**		**7**	
	δ_H (*J* in Hz)	δ_C	δ_H (*J* in Hz)	δ_C
1		155.4		155.4
2		106.0		105.8
3		163.5		163.3
4	6.53, s	91.4	6.50, s	91.4
4a		158.9		158.8
5	6.71, s	103.1	6.67, s	101.2
6		153.5		153.3
7		139.5		140.5
8		121.3		122.6
8a		111.4		114.3
9		179.1		179.3
9a		108.2		108.4
10a		153.5		153.6
1'	2.89, dd (17.0, 5.5) 2.54, dd (17.0, 7.4)	26.9	2.89, dd (17.0, 5.5) 2.54, dd (17.0, 7.4)	26.9
2'	3.77, t (7.0)	69.4	3.77, t (6.9)	69.4
3'		79.2		79.5
4'	1.33, s	20.6	1.33, s	20.6
5'	1.44, s	25.5	1.45, s	25.5
1''	7.94, d (10.0)	122.4	3.45, t (6.8)	23.8
2''	5.83, d (10.0)	132.9	1.84, t (6.8)	33.9
3''		76.6		75.2
4''	1.46, s	27.1	1.37, s	26.4
5''	1.46, s	27.1	1.37, s	26.6
OCH_3-3	3.93, s	56.5	3.91, s	56.5

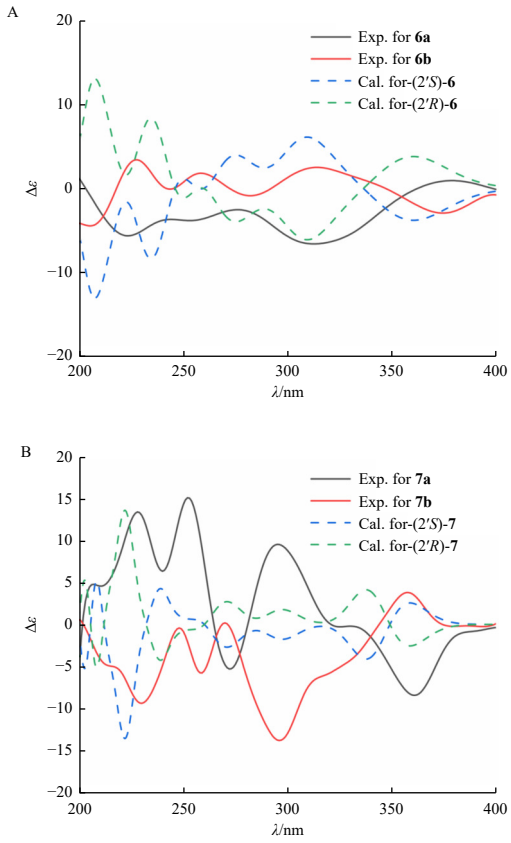

Fig. 3 The experimental and calculated ECD spectra of **6a**/**6b** (A) and **7a**/**7b** (B).

(**20**) [26], gentisein (**21**) [27], 1,3,6-trihydroxy-5-methoxyxanthone (**22**) [28], 1,3,6-trihydroxy-7-methoxyxanthone (**23**) [29], and 1,5,6-trihydroxy-3-methoxy-xanthone (**24**) [30].

The anti-inflammatory effects of all isolated compounds were evaluated on LPS-induced RAW264.7 cells. Cell viability assays indicated that all compounds, except for **2**, **4**, and **5**, exhibited no significant cytotoxicity at concentrations up to 50 μmol·L^{-1}. Subsequently, the inhibition of LPS-stimulated NO production by non-cytotoxic xanthones was assessed using the Griess assay, with dexamethasone (Dex) serving as a positive control. The results revealed that one novel xanthone (**7b**) and two known compounds (**19** and **21**) demonstrated notable anti-inflammatory activities, with IC_{50} values of 16.44 ± 0.69, 14.28 ± 0.78, and 10.67 ± 3.28 μmol·L^{-1}, respectively. The remaining compounds also exhibited dose-dependent inhibition of LPS-stimulated NO production, with IC_{50} values ranging from 18.39 to 50 μmol·L^{-1} (Table 5).

Subsequently, the study evaluated the levels of pro-inflammatory cytokines TNF-α and IL-6. Compounds **7b**, **19**, and **21** demonstrated a significant dose-dependent reduction in the expression of TNF-α and IL-6 (Fig. 4). Notably, the inhibitory effect of compound **21** on IL-6 at 20 μmol·L^{-1} was comparable to that of Dex.

Our results demonstrated that the anti-inflammatory properties of xanthone derivatives were associated with the types of substituents rather than their steric configuration. The study found that compound **11** exhibited higher anti-inflammatory activity compared to compound **12**, suggesting that methylation of the 2-hydroxyl group might reduce activity. Additionally, the introduction of a 2,2-dimethyl-pyran ring decreased inhibitory effects (compounds **13** *vs* **14**, **19** *vs* **21**). This discovery not only expands the diversity of xanthones found in the *Garcinia* genus but also provides promising lead compounds for the development of novel anti-inflammatory agents.

To investigate the pharmacological mechanism, 120 targets were predicted for all isolated compounds using PharmMapper [31-33] (Norm Fit ≥ 0.7, Zscore ≥ 0), while 1347 inflammatory targets were identified from GeneCards [34]. The intersection of compound targets and inflammation targets yielded 47 common targets (Fig. S1A). A protein-protein interaction (PPI) network map was generated using the STRING database (Fig. S1B). Cytoscape software was employed to visualize and analyze the PPI network, which comprised 47 nodes and 312 edges (Fig. S1C). The 47 intersected targets were input into the DAVID [35] database for Gene Ontology (GO) and Kyoto Encyclopedia of Genes and Genomes (KEGG) enrichment analyses. The top 15 significantly enriched terms for biological process (BP), cell component (CC), and molecular function (MF) are presented in Fig. S1D. In BP, the targets were primarily involved in negative regulation of apoptotic process, positive regulation of gene expression, proteolysis, positive regulation of protein kinase B signaling, and positive regulation of mitogen-activated protein kinase (MAPK) cascade. In CC, the targets were mainly associated with the extracellular region, ficolin-1-rich granule lumen, extracellular space, and receptor complex. In MF, the targets were linked to RNA polymerase II transcription factor activity, protein kinase activity, nitric-oxide synthase regulator activity, peptidase activity, and protein serine/threonine/tyrosine kinase activity. Additionally,

Table 4 ^{1}H (600 NMR) and ^{13}C (150 NMR) data of compound **8** (in CD_3OD).

No.	δ_H (*J* in Hz)	δ_C	No.	δ_H (*J* in Hz)	δ_C
1		162.8	9		182.1
2	6.21, s	98.7	9a		103.1
3		165.3	10a		153.7
4		105.6	1'	3.21, dd (13.8, 5.4) 3.08, dd (13.8, 7.4)	29.9
4a		157.0	2'	4.48, t-like (6.4)	76.3
5		133.9	3'		148.8
6		148.1	4'	4.80, brs 4.71, brs	110.9
7	6.87, d, (7.9)	113.6	5'	1.89, s	18.1
8	7.57, d, (7.9)	117.5			
8a		114.6			

Table 5 Inhibitory effects of compounds **1**, **3**, and **6**–**24** on NO production in LPS-induced RAW264.7 cells (mean ± SD, *n* = 3).

Compound	IC_{50}/(μmol·L^{-1})	Compound	IC_{50}/(μmol·L^{-1})
1	> 50	**14**	27.81 ± 1.05
3	27.35 ± 1.80	**15**	29.77 ± 0.21
6a	22.09 ± 1.65	**16**	> 50
6b	21.26 ± 2.08	**17**	31.09 ± 0.90
7a	18.52 ± 0.48	**18**	> 50
7b	16.44 ± 0.69	**19**	14.28 ± 0.78
8	31.55 ± 0.87	**20**	23.09 ± 4.76
9	31.44 ± 1.45	**21**	10.67 ± 3.28
10	44.01 ± 2.96	**22**	20.59 ± 1.36
11	31.74 ± 1.78	**23**	42.71 ± 1.79
12	40.23 ± 1.24	**24**	18.39 ± 1.74
13	43.77 ± 0.69	Dexamethason[a]	9.29 ± 0.80

[a] Positive control.

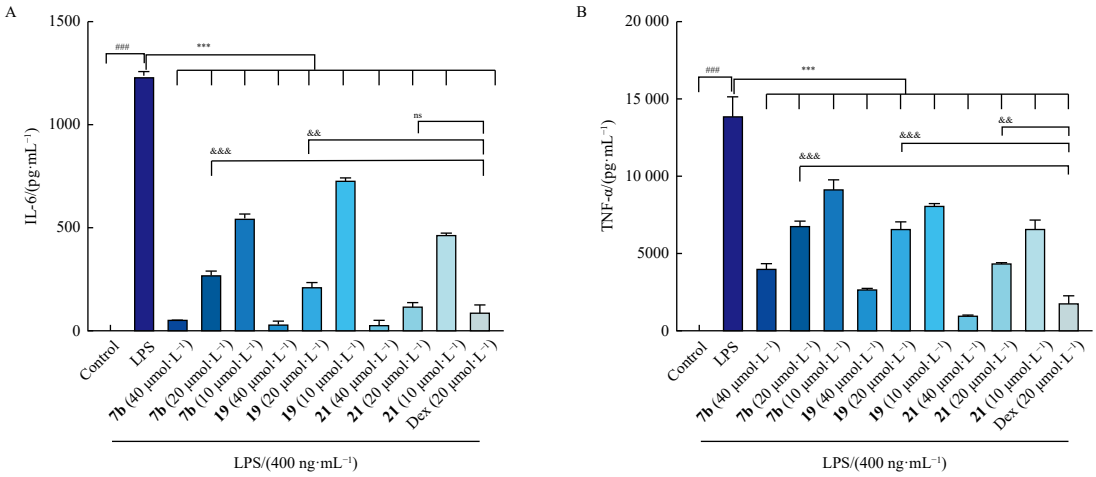

Fig. 4 Effect of compounds **7b**, **19,** and **21** on LPS-induced pro-inflammatory cytokine production (A, IL-6; B, TNF-α) in RAW264.7 cells. $^{###}P < 0.001$ *vs* the control group; $^{***}P < 0.001$ *vs* the LPS-treated group; $^{&}P < 0.05$, $^{&&}P < 0.01$, $^{&&&}P < 0.001$ *vs* the Dex group.

KEGG enrichment analysis identified 97 pathways ($P \leq 0.05$), with the top 15 pathways based on *P*-values illustrated in bubble maps (Fig. S1E). The most relevant pathways included those in cancer, IL-17, MAPK, and EGFR tyrosine kinase inhibitor resistance.

3. Conclusion

In summary, ten previously undescribed and sixteen known xanthones were isolated from *G. pedunculata* and *G. nujiangensis*. This study expands the compound library of *Garcinia*, and further exploration may reveal additional active ingredients with diverse structures in this genus. Furthermore, we evaluated their cell viability and anti-inflammatory properties by measuring the inhibition of NO production in LPS-stimulated RAW264.7 macrophages. Compounds **7b**, **19**, and **21** exhibited significant anti-inflammatory activity and inhibited the release of pro-inflammatory cytokines (TNF-α and IL-6) in a dose-dependent manner. The inhibitory effect of compound **21** on IL-6 at 20 μmol·L^{-1} was comparable to that of the positive control. GO and KEGG enrichment analysis indicated that the overlapped targets were closely associated with major pathogenic processes related to inflammation, including positive regulation of MAPK cascade, protein kinase activity, nitric-oxide synthase regulator activity, MAPK signaling pathway, and EGFR tyrosine kinase inhibitor resistance.

4. Experimental

4.1. General experimental procedures

The HR-ESI-MS spectra were obtained using a Bruker micro-TOFQ-Q mass spectrometer (Bruker BioSpin Co., Billerica, USA). NMR spectroscopic data were recorded on a Bruker AV-600 NMR spectrometer with tetramethylsilane as an internal standard (Bruker BioSpin Co., Billerica, USA). UV spectra were acquired using a Shimadzu UV-2400 spectrometer (Shimadzu, Kyoto, Japan). Optical rotations were measured on an Anton Paar MCP 200 polarimeter (JASCO, Tokyo, Japan). The ECD spectrum was recorded using a Bio-Logic MOS 450 spectrometer (Bio-Logic) MOS 450 spectrometer (Bio-Logic, Seyssinet-Pariset, France). Column chromatography was performed using silica gel (200–300 mesh, Qingdao Haiyang Chemical Co., Ltd., Qingdao, China), octadecylsilyl (ODS, 50 μm, YMC Co., Ltd., Kyoto, Japan), MCI gel (Mitsubishi Chemical Industries Ltd., Tokyo, Japan), and Sephadex LH-20 (Pharmacia Biotech, Uppsala, Sweden). Semi-preparative HPLC was conducted on a COSMOSIL column (250 mm × 10 mm, 5 μm) equipped with an LC-6AD pump and a Shimadzu SPD-20A UV-vis detector (Shimadzu Co., Ltd., Tokyo, Japan). Chiral HPLC was performed on a Daicel Chiralpak IB column (250 mm × 4.6 mm, 5 μm) equipped with an LC-20AB pump and a Shimadzu SPD-M20A UV-vis detector (Shimadzu Co., Ltd., Tokyo, Japan). Thin layer chromatography (TLC) analysis was carried out on silica gel plates (GF254, Qingdao Haiyang Chemical Co., Ltd., Qingdao, China). All organic solvents were purchased from Yuwang and Laibo Chemicals Industries Ltd. (Shenyang, China).

4.2. Plant material

Twigs and leaves of *G. nujiangensis* were acquired from Kunming Plantwise Biotech Co., Ltd. (Kunming, China). The plant material was collected in March 2018 from Namti, Grape County, Kachin Province (GPS, 27°21'N/97°24'E), Myanmar. Mr. Jun Zhang from Kunming Plantwise Biotech Co., Ltd. (Kunming, China) authenticated the samples as *G. nujiangensis*. A voucher specimen (SPU-NJ2018) has been deposited in the Department of Natural Products Chemistry at Shenyang Pharmaceutical University, Shenyang, China.

Leaves of *G. pedunculata* were acquired from Kunming Plantwise Biotech Co., Ltd. (Kunming, China). The specimens were collected in September 2018 from Longchuan County, Dehong Prefecture, Yunnan Province, China (GPS coordinates: 24°18'N/97°79'E). Mr. Jun Zhang of Kunming Plantwise Biotech Co., Ltd. (Kunming, China) authenticated the samples as *G. pedunculata*. A voucher specimen (SPU-GP2018) has been deposited in the Department of Natural Products at Shenyang Pharmaceutical University, Shenyang, China.

4.3. Extraction and isolation

The air-dried twigs and leaves of *G. nujiangensis* (20.0 kg) were extracted with an acetone/water mixture (80∶20) (*V/V*, 30 L) at room temperature for three days, repeating the process three times. The resulting crude acetone extract underwent successive partitioning using petroleum ether (PE), dichloromethane (CH_2Cl_2), ethyl acetate (EtOAc), and *n*-butanol (*n*-BuOH), yielding corresponding PE, CH_2Cl_2, EtOAc, and *n*-BuOH extracts.

The EtOAc extracts (890 g) were subjected to silica gel CC eluted with CH_2Cl_2/CH_3OH (100∶0–0∶100, *V/V*) to yield eight fractions (E1–E8). Fraction E4 (189 g) was further subjected to silica gel CC eluted with CH_2Cl_2/CH_3OH (100∶0–0∶100, *V/V*), resulting in seventeen fractions (E4A–E4Q). Subfraction E4F was separated by Sephadex LH-20 to produce four subfractions (E4F1–E4F4). Subfraction E4F2 was purified using hemi-prepar-

ative HPLC (CH_3CN/H_2O 51∶49, *V/V*; flow rate, 2.0 mL·min^{-1}) to obtain **24** (2.9 mg, t_R = 22.5 min). Subfraction E4G underwent silica gel CC elution with CH_2Cl_2/CH_3OH (100∶0–0∶100, *V/V*) and HPLC (CH_3OH–H_2O 65∶35, *V/V*; flow rate, 2.0 mL·min^{-1}), ultimately yielding **18** (1.1 mg, t_R = 143 min). Subfraction E4H was separated by MCI CC (MeOH–H_2O, 10∶90–100∶0, *V/V*) to obtain four subfractions (E4H1–E4H4). E4H3 was purified by Sephadex LH-20 CC and HPLC (CH_3OH–H_2O 52∶48, *V/V*; flow rate, 2.0 mL·min^{-1}) to yield **8** (3.0 mg, t_R = 85.4 min).

The air-dried leaves of *G. pedunculata* (9.8 kg) were powdered and then extracted with acetone/water (80∶20, *V/V*, 30 L, three days per time) at room temperature three times. The acetone crude extracts were subjected to a silica gel column eluted with PE, CH_2Cl_2, EtOAc, and MeOH to yield four fractions (A–D).

Fraction B underwent separation using a silica gel column eluted with purified by preparative TLC (PE/EtOAc) (100∶0–0∶100, *V/V*), yielding seven subfractions, B1–B7. **9** (53.0 mg) and **11** (1.46 mg) were isolated through recrystallization from fraction B2. Fraction B3 was subjected to ODS CC (MeOH/H_2O, 40∶60–100∶0, *V/V*), resulting in nine subfractions (B3A–B3I). Fraction B3E was further purified by HPLC (CH_3OH/H_2O 90∶10, *V/V*; flow rate, 2.0 mL·min^{-1}), yielding **10** (3.3 mg, t_R = 73.9 min) and **3** (1.2 mg, t_R = 34.3 min). HPLC separation of fraction B3F (CH_3OH/H_2O 90∶10, *V/V*; flow rate, 2.0 mL·min^{-1}) produced **1** (1.9 mg, t_R = 66.7 min). Fraction B3G underwent Sephadex LH-20 CC, resulting in three subfractions (B3G1–B3G3). Fraction B3G2 was purified by preparative TLC (PE/EtOAc, 3∶1) to obtain **12** (1.2 mg). ODS CC (MeOH/H_2O, 40∶60–100∶0, *V/V*) of fraction B4 yielded six subfractions (B4A–B4D). Fraction B4C underwent Sephadex LH-20 CC and HPLC (CH_3OH/H_2O 62∶38, *V/V*; flow rate, 2.0 mL·min^{-1}), producing **13** (3.9 mg, t_R = 34.6 min). MCI CC (MeOH/H_2O, 40∶60–100∶0, *V/V*) of fraction B5 resulted in nine subfractions (B5A–B5I). Sephadex LH-20 CC and HPLC (CH_3OH/H_2O 60∶40, *V/V*; flow rate, 2.0 mL·min^{-1}) purification of fraction B5E yielded **21** (1.7 mg, t_R = 26.3 min). ODS CC (MeOH/H_2O, 30∶70–100∶0, *V/V*) of fraction B5F produced seven subfractions (B5F1–B5F7). HPLC separation (CH_3OH/H_2O, 80∶20, *V/V*; flow rate, 2.0 mL·min^{-1}) of fraction B5F5 yielded **5** (1.1 mg, t_R = 42.5 min). Fraction B5G underwent silica gel column chromatography with PE/EtOAc (100∶0–0∶100, *V/V*), resulting in nine subfractions, B5G1–B5G9. HPLC purification (CH_3OH/H_2O, 75∶25, *V/V*; flow rate, 2.0 mL·min^{-1}) of fraction B5G2 yielded **15** (7.7 mg, t_R = 27.1 min). HPLC separation (CH_3OH/H_2O, 69∶31, *V/V*; flow rate, 2.0 mL·min^{-1}) of fraction B5G5 produced **19** (6.9 mg, t_R = 51.8 min). Sephadex LH-20 CC and HPLC (CH_3OH/H_2O, 71∶29, *V/V*; flow rate, 2.0 mL·min^{-1}) of fraction B5G6 yielded **14** (2.0 mg, t_R = 90.9 min) and **16** (2.0 mg, t_R = 93.6 min). Sephadex LH-20 CC and HPLC purification (CH_3OH/H_2O, 75∶25, *V/V*; flow rate, 2.0 mL·min^{-1}) of fraction B5G7 resulted in **17** (5.4 mg, t_R = 50.0 min).

Fraction C was separated using a silica gel column eluted with CH_2Cl_2/CH_3OH (100∶0–0∶100, *V/V*) to yield nine subfractions, C1–C9. Fraction C2 underwent MCI CC (CH_3OH/H_2O, 10∶90–100∶0, *V/V*) to produce five subfractions, C2A–C2E. Fractions C2B and C2C were purified *via* HPLC (CH_3OH/H_2O, 83∶17, *V/V*; flow rate, 2.0 mL·min^{-1}) to obtain **4** (3.5 mg, t_R = 43.1 min) and **2** (2.3 mg, t_R = 60.5 min), respectively. Fraction C4 underwent silica gel column chromatography eluted with CH_2Cl_2/CH_3OH (100∶0–0∶100, *V/V*) to generate six subfractions, C4A–C4F. Fraction C4B was purified using Sephadex LH-20 CC and HPLC (CH_3OH/H_2O 54∶46, *V/V*; flow rate, 2.0 mL·min^{-1}) to yeild **22** (1.6 mg, t_R = 69.3 min) and **20** (2.7 mg, t_R = 71.7 min). Fraction C4C underwent HPLC purification (CH_3CN/H_2O 46∶54, *V/V*; flow rate, 2.0 mL·min^{-1}) to produce **23** (2.2 mg, t_R = 29.3 min). Fraction C4E was purified using Sephadex LH-20 to generate two subfractions, C4E1–C4E2. Fraction C4E1 underwent HPLC separation (CH_3CN/H_2O 57∶43, *V/V*; flow rate, 2.0 mL·min^{-1}) to yeild **6** (3.4 mg, t_R = 33.2 min) and **7** (4.5 mg, t_R = 36.5 min). **6** and **7** were further separated by chiral HPLC (hexane/ethanol 89∶11, *V/V*; flow rate, 0.5 mL·min^{-1}) to obtain **6a** (1.81 mg, t_R = 34.4 min), **6b** (1.5 mg, t_R = 37.3 min), **7a** (2.33 mg, t_R = 28.7 min) and **7b** (2.03 mg, t_R = 32.0 min), respectively.

Garpedunxanthone A (**1**): pale yellow amorphous powder; UV (CH_3OH) λ_{max} (log ε) 262 (4.14), 283 (4.20), 350 (4.18) nm; ^1H and ^{13}C NMR data see Tables 1 and 2; HR-ESI-MS *m/z* 389.1025 $[M - H]^-$ (Calcd. for $C_{23}H_{17}O_6$, 389.1025).

Garpedunxanthone B (**2**): yellow needle crystal; UV (CH_3OH) λ_{max} (log ε) 284 (3.97), 306 (3.85), 337 (3.87) nm; ^1H and ^{13}C NMR data (Tables 1 and 2); HR-ESI-MS *m/z* 351.0863 $[M + H]^+$ (Calcd. for $C_{20}H_{15}O_6$, 351.0869).

Garpedunxanthone C (**3**): pale yellow amorphous powder; UV (CH_3OH) λ_{max} (log ε) 290 (3.93), 338 (3.42), 373 (3.31); ^1H and ^{13}C NMR data (Tables 1 and 2); HR-ESI-MS *m/z* 395.1489 $[M + H]^+$ (Calcd. for $C_{23}H_{23}O_6$, 395.1495).

Garpedunxanthone D (**4**): pale yellow amorphous powder; UV (CH_3OH) λ_{max} (log ε) 292 (4.08), 336 (3.66) nm; ^1H and ^{13}C NMR data (Tables 1 and 2); HR-ESI-MS *m/z* 451.1403 $[M - H]^-$ (Calcd. for $C_{25}H_{23}O_8$, 451.1393).

Garpedunxanthone E (**5**): pale yellow amorphous powder; UV (CH_3OH) λ_{max} (log ε) 279 (3.99), 393 (3.71) nm; ^1H and ^{13}C NMR data (Tables 1 and 2); HR-ESI-MS *m/z* 407.1131 $[M - H]^-$ (Calcd. for $C_{23}H_{20}O_6$, 407.1131).

Garpedunxanthone F (**6**): yellow amorphous powder; UV (CH_3OH) λ_{max} (log ε) 244 (4.15), 262 (4.11), 317 (4.00), 369 (3.51) nm; ^1H and ^{13}C NMR data (Table 3); HR-ESI-MS *m/z* 425.1595 $[M + H]^+$ (Calcd. for $C_{24}H_{25}O_7$, 425.1600). (+) Garpedunxanthone F (**6a**): $[\alpha]_D^{20}$ +52 (*c* 0.16, CH_3OH). ECD (MeOH) λ_{max} (log ε) 223 (−2.12), 275 (−1.78), 312 (−2.19), 379 (1.34) nm. (−) Garpedunxanthone F (**6b**): $[\alpha]_D^{20}$ −35 (*c* 0.22, CH_3OH); ECD (MeOH) λ_{max} (log ε) 244 (4.15), 262 (+1.61), 314 (1.80), 374 (−1.87) nm.

Garpedunxanthone G (**7**): yellow amorphous powder; UV (CH_3OH) λ_{max} (log ε) 256 (4.27), 306 (4.00), 352 (3.72) nm; ^1H and ^{13}C NMR data (Table 3); HR-ESI-MS *m/z* 427.1751 $[M + H]^+$ (Calcd. for $C_{24}H_{25}O_7$, 427.1757). (+) Garpedunxanthone G (**7a**): $[\alpha]_D^{20}$ +11 (*c* 0.20, CH_3OH); ECD (MeOH) λ_{max} (log ε) 238 (+0.59), 287 (+1.70), 322 (+1.59), 356 (−2.21) nm. (−) Garpedunxanthone G (**7b**): $[\alpha]_D^{20}$ −43 (*c* 0.16, CH_3OH); ECD (MeOH) λ_{max} (log ε) 252 (+1.60), 294 (−1.90), 359 (+2.03) nm.

Nujiangxanthone Q (**8**): yellow amorphous powder; UV (CH_3OH) λ_{max} (log ε) 252 (3.69), 327 (3.40) nm. ^1H and ^{13}C NMR data (Table 4); HR-ESI-MS *m/z* 343.0819 $[M - H]^-$ (Calcd. for $C_{18}H_{15}O_7$, 343.0818).

4.4. Electronic circular dichroism (ECD) calculation

The compound structures were utilized to search for conformers using Spartan 14.0 (Wavefunction Inc., Irvine, CA, USA) under the MMFF force field. The low-energy conformers were initially optimized in the gas phase using a semi-empirical method in the Gaussian 09 program package. These optimized structures were further refined and analyzed using density functional theory (DFT) at the B3LYP/6-31G (d, p) level, resulting in no imaginary frequencies. Subsequently, the ECD spectra were calculated using TD-DFT-B3LYP/6-31G (d, p) level in methanol solution. Finally, the calculated low-energy conformational results were Boltzmann averaged using SpecDis1.51 software to generate the depicted ECD spectra of the compound.

4.5. Anti-inflammatory assay

(1) Cell culture: RAW264.7 macrophage cells were obtained from American Type Culture Collection (ATCC, Manassas, VA,

USA) and cultured in DMEM medium (Vivacell Bio, Shanghai, China) supplemented with 12% fetal bovine serum (FBS, Vivacell Bio, Shanghai, China) and 1% penicillin-streptomycin solution (Vivacell Bio, Shanghai, China). The cells were maintained in a humidified incubator at 37 °C with 5% CO_2.

(2) Cell viability assay: RAW264.7 cells were seeded into 96-well plates at a density of 5 × 10^4 cells per well and cultured for 18 h. The cells were then treated with compounds (**1**–**24**) for 24 h. Subsequently, 10 μL of CCK8 reagent (APExBIO, Houston, USA) was added to each well, followed by incubation for 1 h. The absorbance was measured using a microplate reader at a wavelength of 450 nm. Each sample was tested in triplicate.

(3) Assay of the production of NO: the cells (5 × 10^4 cells/well, 100 μL medium/well) were cultured for 18 h in a 96-well plate. Subsequently, in the presence or absence of LPS (Beyotime Biotech, Suzhou, China), a series of concentrations of compounds (**1**, **3**, **6**–**24**) were applied for 24 h. NO levels were detected following the manufacturer's instructions (Beyotime Biotech, Suzhou, China). Dexamethasone (Aladdin, Shanghai, China) served as a positive control. Statistical analyses were performed using GraphPad Prism 9. Each sample was tested in triplicate.

(4) Enzyme-linked immunosorbent assay (ELISA) assays: the cells (1 × 10^6 cells/well, 2 mL medium/well) were cultured for 12 h in a 6-well plate. Subsequently, in the presence or absence of LPS, a series of concentrations of compounds (**7b**, **19**, **21**) were applied for 24 h. The levels of TNF-α and IL-6 were measured according to the manufacturer's instructions (Proteintech, Wuhan, China). Dexamethasone (Aladdin, Shanghai, China) served as a positive control. Statistical analyses were performed using GraphPad Prism 9. Each sample was tested in triplicate.

4.6. Network pharmacological analysis

Potential targets of all isolated constituents were identified using PharmMapper (http://lilab-ecust.cn/). The keyword "Anti-inflammatory" was employed to retrieve disease targets from the GeneCards database (https://www.genecards.org/). The bioinformatics database (https://www.bioinformatics.com.cn/) was utilized to identify overlapping genes between compound targets and inflammation targets. The STRING database facilitated the construction of PPI. All network analyses were conducted using Cytoscape v3.9.1. The DAVID database (https://david.ncifcrf.gov/) was employed for GO analysis and KEGG pathway enrichment.

Availability of supporting information

Supporting information for this work can be obtained by contacting the corresponding authors *via* E-mail.

Declaration of competing interest

These authors have no conflict of interest to declare.

References

1 Medzhitov R. Inflammation 2010: new adventures of an old flame. *Cell*. 2010;140(6):771-776. https://doi.org/10.1016/j.cell.2010.03.006.
2 Das D, Sarkar S, Wann SB, et al. Current perspectives on the anti-inflammatory potential of fermented soy foods. *Food Res Int*. 2022;152:110922. https://doi.org/10.1016/j.foodres.2021.110922.
3 Zhang XY, Lian XY, Li HL, et al. Taxifolin attenuates inflammation via suppressing MAPK signal pathway *in vitro* and *in silico* analysis. *Chin Herb Med*. 2022;14(4):554-562. https://doi.org/10.1016/j.chmed.2021.03.002.
4 Guha S, Majumder K. Structural-features of food-derived bioactive peptides with anti-inflammatory activity: A brief review. *J Food Biochem*. 2019;43(1):e12531. https://doi.org/10.1111/jfbc.12531.
5 Zhu Y, Zhu M, Lance P. INOS signaling interacts with COX-2 pathway in colonic fibroblasts. *Exp Cell Res*. 2012;318:2116-2127. https://doi.org/10.1016/j.yexcr.2012.05.027.
6 Zou DL, Liu FS; Liu L, *et al*. Cytotoxic xanthones from *Garcinia pedunculata* fruits. *Phytochemistry*. 2024;217:113898. https://doi.org/10.1016/j.phytochem.2023.113898.
7 Nhan NT, Nguyen PH, Tran MH, et al. Anti-inflammatory xanthone derivatives from *Garcinia delpyana*. *J Asian Nat Prod Res*. 2021;23:414-422. https://doi.org/10.1080/10286020.2020.1767079.
8 Maharana L, Sethi MK, Dash RN, et al. Evaluation of antidiabetic and antihyperlipidemic effect of *Vernonia divergens* in streptozotocin-induced diabetic rats. *Asian J Pharm Clin Res*. 2019;12(5):104-110. https://doi.org/10.22159/ajpcr.2019.v12i5.32301.
9 Bhattacharjee S, Devi R. A comprehensive review of *Garcinia pedunculata* Roxb. and its therapeutic potential. *Mini-Rev Med Chem*. 2021;21:3113-3143. https://doi.org/10.2174/1389557521666210217094152.
10 Sukandar ER, Kaennakam S, Raab P, et al. Cytotoxic and anti-inflammatory activities of dihydroisocoumarin and xanthone derivatives from *Garcinia picrorhiza*. *Molecules*. 2021;26:6626. https://doi.org/10.3390/molecules26216626.
11 Afzai M, Al-Hassan IM, Al-Masad N. New linear pyhanoxantiionoss from *Calophyllum apetalum*. *Heterocycles*. 1979;12:269. https://doi.org/10.3987/R-1979-02-0269.
12 Kwon J, Hiep NT, Kim D, et al. Neuroprotective xanthones from the root bark of *Cudrania tricuspidate*. *J Nat Prod*. 2014;77:1893-1901. https://doi.org/10.1021/np500364x.
13 Liang X, Hu Y, Li J, et al. Identification and pharmacokinetics of quinone reductase 2 inhibitors after oral administration of *Garcinia mangostana* L. extract in rat by LC–MS/MS. *J Agric Food Chem*. 2020;68:11975-11986. https://doi.org/10.1021/acs.jafc.0c04439.
14 Yang RY, Li P, Li NN, et al. Xanthones from the pericarp of *Garcinia mangostana*. *Molecules*. 2017;22:683. https://doi.org/10.3390/molecules22050683.
15 Zhou XJ, Huang RM, Hao J, et al. Two new prenylated xanthones from the pericarp of *Garcinia mangostana*. *Helv Chim Acta*. 2011;94:2092-2098. https://doi.org/10.1002/hlca.201100157.
16 Liu QY, Li D, Wang AQ, et al. Nitric oxide inhibitory xanthones from the pericarps of *Garcinia mangostana*. *Phytochemistry*. 2016;131:115-123. https://doi.org/10.1016/j.phytochem.2016.08.007.
17 Mkounga P, Fomum ZT, Michèle Meyer, et al. Globulixanthone F, a new polyoxygenated xanthone with an isoprenoid group and two antimicrobial biflavonoidsfrom the stem bark of *Symphonia globulifera*. *Nat Prod Commun*. 2009;4:803-808. https://doi.org/10.1007/s00044-008-9136-x.
18 Cheng HC, Wang LT, Khalil AT, et al. Pyranoxanthones from *Calophyllum inophyllum*. *J Chin Chem Soc*. 2004;51:431-435. https://doi.org/10.1002/jccs.200400066.
19 Panthong K, Pongcharoen W, Phongpaichit S, et al. Tetraoxygenated xanthones from the fruits of *Garcinia cowa*. *Phytochemistry*. 2006;67:999-1004. https://doi.org/10.1016/j.phytochem.2006.02.027.
20 Sen AK, Sarkar KK, Mazumder PC, et al. The structures of garcinones A, B and C: three new xanthones from *Garcinia mangostana*. *Phytochemistry*. 1982;21(7):1747-1750. https://doi.org/10.1016/S0031-9422(82)85052-8.
21 Cortez DAG, Young MCM, Marston A, et al. Xanthones, triterpenes and a biphenyl from *Kielmeyeera coriacea*. *Phytochemistry*. 1998;47(7):1367-1374. https://doi.org/10.1016/S0031-9422(97)00731-0.
22 Sordat DI, Marston A, Hamburger M, et al. Prenylated xanthones from *Garcinia livingstonei*. *Planta Med*. 1989;55:584-584. https://doi.org/10.1016/0031-9422(91)83061-O.
23 Zhang ZZ, ElSohly HN, Jacob MR, et al. Natural products inhibiting *candida Albicans* secreted aspartic proteases from *Tovomita krukovii*. *Planta Med*. 2002;68:49-54. https://doi.org/10.1055/s-2002-20049.
24 Ito C, Miyamoto Y, Nakayama M, et al. A novel depsidone and some new xanthones from *Garcinia* species. *Chem Pharm Bull*. 1997;45(9):1403-1413. https://doi.org/10.1248/cpb.45.1403.
25 Liu XJ, Hu X, Peng XH, et al. Polyprenylated xanthones from the twigs and leaves of *Garcinia nujiangensis* and their cytotoxic evaluation. *Bioorg Chem*. 2020;94:103370. https://doi.org/10.1016/j.bioorg.2019.103370.
26 Frahm AW, Chaudhuri RK. ^{13}C NMR spectroscopy of substituted xanthones-Ⅱ: 13C NMR spectral study of polyhydroxy xanthones. *Tetrahedron*. 1979;35(17):2035-2038. https://doi.org/10.1016/S0040-4020(01)88974-2.
27 Na Z, Xu YK. Chemical constituents from twigs of *Garcinia xipshuanbannaensis*. *Chin J Chin Mater Med*. 2009;34(18):2338-2342.
28 Sabphon C. Cholinesterase inhibitory activities of xanthones from *anaxagorea luzonensis* A. gray. *J Med Plant Res*. 2012;6(21):3781-3785. https://doi.org/10.5897/JMPR12.346.
29 Ghosal S, Chaudhuri RK, Nath A. Chemical constituents of gentianaceae IV: new xanthones of *Canscora decussata*. *J Pharm Sci*. 1973;62:137-139. https://doi.org/10.1002/jps.2600620128.
30 Terreaux C, Maillard M, Gupta MP, et al. Xanthones from *Schultesia lisianthoides*. *Phytochemistry*. 1995;40:1791-1795. https://doi.org/10.1016/0031-9422(95)00483-N.
31 Liu X, Ouyang S, Yu B, et al. PharmMapper server: a web server for potential drug target identification *via* pharmacophore mapping approach. *Nucleic Acids Res*. 2010;38:609-614. https://doi.org/10.1093/nar/gkq300.
32 Wang X, Pan C, Gong J, et al. Enhancing the enrichment of pharmacophore-based target prediction for the polypharmacological profiles of drugs. *J Chem Inf Model*. 2016;56:1175-1183. https://doi.org/10.1021/acs.jcim.5b00690.
33 Wang X, Shen Y, Wang S, et al. PharmMapper 2017 update: a web server for potential drug target identification with a comprehensive target pharmacophore database. *Nucleic Acids Res*. 2017;45:356-360. https://doi.org/10.1093/nar/gkx374.
34 Stelzer G, Rosen N, Plaschkes I, *et al*. The GeneCards suite: from gene data mining to disease genome sequence analyses. *Curr Protoc Bioinformatics*. 2016;54:1.30.1-1.30.33. https://doi.org/10.1002/cpbi.5.
35 Huang DW, Sherman BT, Lempicki RA. Systematic and integrative analysis of large gene lists using DAVID bioinformatics resources. *Nature Protoc*. 2009;4:44-57. https://doi.org/10.1038/nprot.2008.211.